JOURNAL OF GEOPHYSICAL RESEARCH, VOL. 89, NO. B10, PAGES 8269–8285, SEPTEMBER 30, 1984

Hydrodynamic Aspects of Caldera-Forming Eruptions: Numerical Models

K. H. WOHLETZ, T. R. MCGETCHIN,[1] M. T. SANDFORD II, AND E. M. JONES

Earth and Space Sciences Division, Los Alamos National Laboratory

Comparison of results from a two-dimensional numerical eruption simulation (KACHINA) to calculations based upon a shock tube analog supports the conclusion that the hydrodynamics during the initial minutes of large caldera-forming ash flow eruptions may be dominated by blast wave phenomena. Field evidence for this phenomenology is pyroclastic surge deposits commonly occurring both directly below caldera-related ash flow sheets, on top of a preceding Plinian fall deposit (ground surge), and separating individual ash flow units. We model the eruption of the Tshirege member of the Bandelier Tuff (1.1 Ma B.P.) from the Valles caldera, New Mexico. In the model a magma chamber at 100 MPa (1 kbar) and 800°C is volatile rich, with an average H_2O abundance above saturation greater than 8.7 wt % increasing to nearly 100 wt % near the very top of the chamber. Using a shock tube analogy, decompression of the chamber through a wide-open dikelike vent 0.1 km wide and 1 to 5 km long forms a shock wave of 3 MPa ($\simeq$30 atm) with a velocity greater than 1.0 km s^{-1}. Steady flow of material erupted from the vent begins after 20 to 100 s based upon a 7-km depth from the ground surface to a reflective (density) boundary in the chamber and a rarefaction wave velocity of 100 to 600 m s^{-1}. The velocity of the ash front behind the shock wave is 300 to 500 m s^{-1}. The shock tube model serves as a basis to evaluate the consistency of the KACHINA code results which are similar to a one-dimensional problem along the symmetry axis. The results of the KACHINA simulation show in some detail the effect of multiple reservoir rarefaction reflections and possibly Prandtl-Meyer expansion in generating compressive wave fronts following the initial shock. The rarefaction resonance not only prolongs unsteady flow in the vent but tends to promote surging flow of ash behind the leading shock. Furthermore, these results are consistent with a blast wave characterized as a shock front followed by one or more pulses of entrained ash. The blast wave shocks ambient air to higher pressures and temperatures, the magnitudes of which depend strongly on the initial chamber overpressure, distance, and direction from the vent. In consideration of volcanic hazards our numerical model shows that a shock wave compressed the atmosphere to pressures of $\simeq$0.2 to 0.7 MPa (2–7 atm) and temperatures of $\simeq$200° to 300°C for distances to 10 km from the Bandelier vent(s).

INTRODUCTION

Plinian eruption is widely recognized to be associated with the most explosive volcanic activity on earth. Plinian activity encompasses a wide range of phenomena and energetics [*MacDonald*, 1972] including most notably a high-volume rate of ejection, widespread distribution of pumice and ash as flows and falls, and associated caldera collapse. A recent more specific definition of the term Plinian [*Walker*, 1981] restricts its application to the pumice and ash fall phase of eruption during which a high (10–50 km) eruption column is sustained and volume flux is greater than 10^6 m^3 s^{-1}. However, the original general descriptions published by Pliny the Younger of Vesuvius explosive eruptions (as in A.D. 79) are now known to include eruptive activity responsible for emplacement of the pyroclastic flow and surge accompanying the fall deposits [*Rosi and Santacroce*, 1983; *Sheridan et al.*, 1981]. The importance of the surge accompanying fall and flow deposits has been illustrated by *Sparks et al.* [1973] and is well documented for the Bandelier Tuff (Valles caldera) by *Fisher* [1979]. Figure 1 shows a similar relationship for the Bishop Tuff (Long Valley caldera) which has been mentioned by *Wohletz and Sheridan* [1979]. Although this stratigraphic sequence may not strictly characterize caldera-related pyroclastic deposits, it is strong evidence for a multistage eruption and supports the original, more general definition we follow for the term.

Assuming that pyroclastic surges characterize deposits following "blast" phenomena where highly unsteady flow and shock wave propagation can be inferred [*Glasstone and Dolan*, 1977; *Hoblitt et al.*, 1981; *Kieffer*, 1981], we characterize caldera-forming eruptions of the Plinian type by four stages: (1) the initial vent-opening phase during which a column is formed and pumice fall deposits result; (2) the blast phase during which the vent widens, allowing communication of acoustic waves from the magma chamber to the atmosphere, and unsteady fluid flow occurs owing to sudden release of confining pressure on the volatile-rich top of a magma chamber; (3) the gradual decompression phase consisting of nearly steady flow of vapor and ash which depletes the volatile-charged portion of the chamber; and finally (4) the phase of passive extrusion of the viscous incompressible lava. Stage 2, the blast phase, corresponds to the transition from *Walker*'s [1981] Plinian fall eruption to emplacement of ash flow deposits. Hence it may characterize the onset of column collapse and in some situations blast waves also accompany initial vent opening. It is likely that blast occurs whenever highly unsteady flow conditions occur in the vent and materials are accelerated to velocities greater than the speed of sound in the atmosphere. *Wilson et al.* [1980] and *Sparks et al.* [1978] discuss and model the steady flow characteristics of Plinian column activity and the production of ash flows by column collapse. Other useful contributions to eruption modeling are those of *McGetchin and Ullrich* [1973], *Pai et al.* [1978], and *Eichelberger and Hayes* [1982].

This paper is directed at the blast phase of the large eruption which likely initiated the emplacement of the Bandelier Tuff ash flow from the 20-km-wide Valles caldera, New Mexico, over 1 m.y. ago [*Fisher*, 1979; *Smith and Bailey*,

[1] Deceased.

Paper number 4B0367.

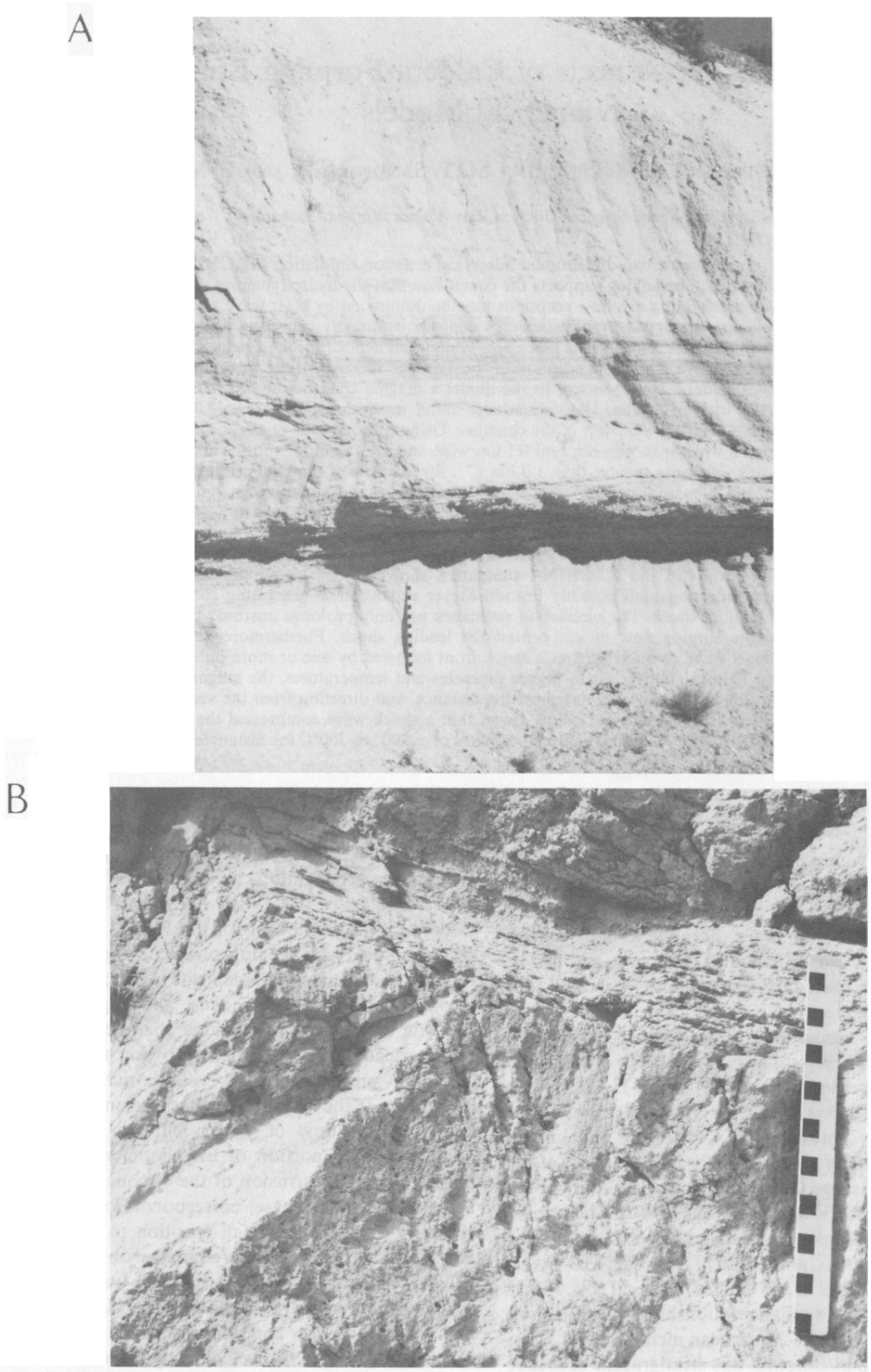

Fig. 1. Photographs of the Bishop Tuff. (*a*) A lower tuff section exposed in a quarry north of Bishop shows a characteristic pyroclastic flow stratigraphy of Plinian pumice fall deposits overlain by pyroclastic surge and flow. Meter stick for scale. (*b*) Crystal-rich, undulating, sandy partings typically mark the contact between pyroclastic flow units. These finely bedded partings are probably a type of surge deposit and may represent a blast eruption preceding emplacement of a pyroclastic flow unit or an unsteady phase during pyroclastic flow eruption.

1961]. We compare a simple one-dimensional shock tube model [*Wright*, 1967] with two-dimensional numerical results from KACHINA which makes a computer solution of the Eulerian hydrodynamic equations for two-phase flow [*Amsden and Harlow*, 1974]. The shock tube analog to volcanic eruptions was first suggested by *Bennett* [1971], and we believe it is an adequate physical model by which we can evaluate results of the more detailed KACHINA calculations [*Sandford et al.*, 1975].

The main problems of modeling this explosive phenomen-

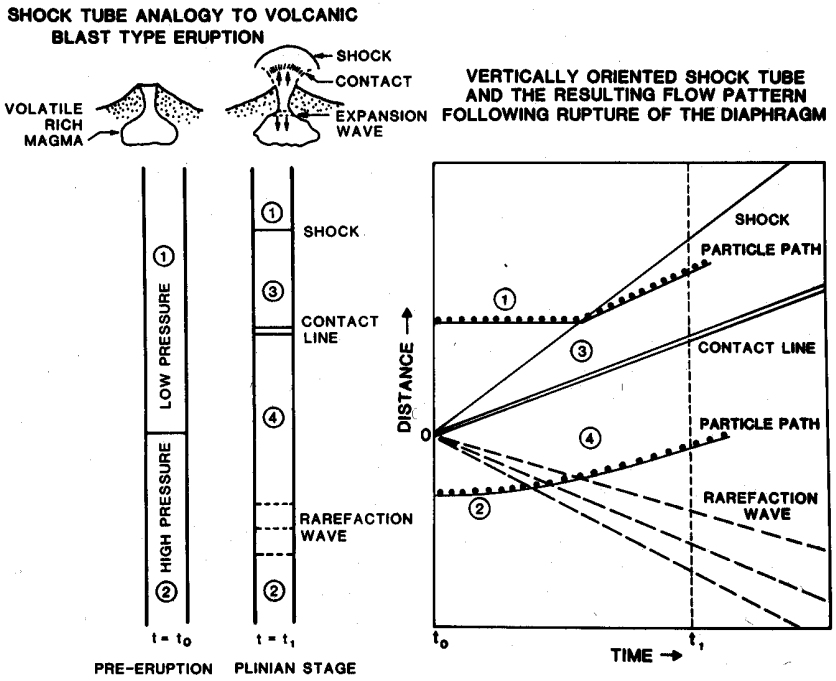

Fig. 2. A sketch of the gas dynamic shock tube analogy used to interpret a volcanic blast in the vertical direction. The one-dimensional configuration of a shock tube before and after bursting and an ideal distance-time plot for the shock wave, contact line, and rarefaction wave are shown. Low-pressure and high-pressure materials are designated 1 and 2; shocked low-pressure material, 3; and rarefied high-pressure material, 4.

ology are that important physical constraints such as sound speed and an equation of state for magma steam systems, water vaporization rate, and observational accounts as to the duration of large caldera-forming Plinian eruptions are not known. Several important parameters that determine the phenomena of Plinian eruption include the geometry, depth, and volume of the magma chamber; the temperature and pressure distribution throughout the chamber; the equation of state (e.g., compressibility) and the amount of volatile substances in the magma; and vent size and geometry. These unknown parameters can be calculated from theory with some certainty and adjusted for a specific volcano, as for the Valles caldera discussed below.

Shock Tube Model

Although no large Plinian eruptions of the size that erupted the Bandelier Tuff have been scientifically witnessed, the phenomenology of the eruption and its effects can be quantitatively modeled. The fact that some large eruptions may be initiated by a blast prior to the more continuous emission of tephra and gases has been shown by the May 1980 eruption of Mount St. Helens [*Kieffer*, 1981]. Assuming that a high-pressure magma chamber is separated from the atmosphere prior to eruption and that there is a nearly instantaneous failure of the rock overburden capping the chamber, an initial blast phase is predictable using shock tube theory. The configuration of a typical shock tube (Figure 2) consists of two chambers separated by a diaphragm. One chamber is filled with high-pressure gas, and the other is evacuated or filled with low-pressure gas. When the diaphragm ruptures, a high-velocity flow ensues that "equilibrates" the two chambers. The subsequent condition of the gas is uniquely determined by the constitutive relations for the gas and by the initial pressure difference. Thus we consider the blast phase to involve the unsteady flow conditions that occur during the time the rarefaction wave travels down into the magma chamber where it reflects and moves back to the surface. Shock tubes have been well studied and are commonly used to generate the high-speed flows required for aeronautical engineering [*Wright*, 1967].

In order to apply shock tube theory to the blast phase of an explosive eruption, a few important and fundamental constraints need to be specified. First, the magma chamber overpressure is estimated from the physical properties of rock and by petrologic considerations. Assuming the magma chamber walls are strong, the overburden exerts a lithostatic pressure which varies with depth, assuming negligible tensile strength of the overburden. The tops of large silicic magma chambers typically reside within $\simeq 3$ to 10 km of the earth's surface, which corresponds to pressures of 100 to 300 MPa (1 to 3 kbar). This pressure is also predicted for the salic ternary minima compositions [*Tuttle and Bowen*, 1958] noted for silicic magmas containing H_2O erupted from calderas. For our model we assume an overburden thickness of the order of 3 to 4 km corresponding to a reservoir pressure of about 100 MPa.

A second critical constraint is the equation of state of the material at the top of the magma chamber. Assuming the top of the chamber to be a volatile-rich mixture of compressible water and incompressible silicate melt, the pressure-volume relations of the mixture reflect those of the water fraction (which is not in solution with the melt). Figure 3 shows isothermal pressures for the specific volume of the mixture at different temperatures. This model assumes a simple mixture of incompressible melt with density 2.5×10^3 kg m^{-3} at 800°C and water with a specific volume [*Burnham et al.*, 1969] multiplied by its weight percent in the mixture. For example, with no water present the specific volume of the melt is constant with changing pressure at 0.4×10^{-3} m^3 kg^{-1}. At 100 MPa and 5 wt % water in a free phase (4.2×10^{-3} m^3 kg^{-1}), the specific volume of the mixture is 0.6×10^{-3} m^3 kg^{-1} and the water volume fraction is 36%. Clearly, the water volume fraction increases with decreasing pressure.

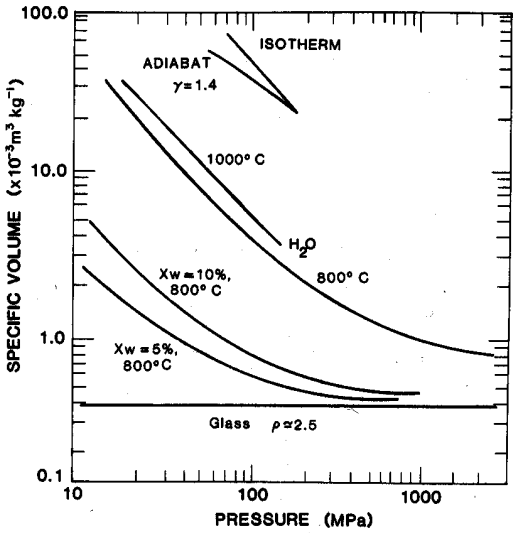

Fig. 3. The pressure-volume diagram for water and melt mixtures based upon the equation of state of water at 800°C and a constant melt (glass) density of 2.5×10^3 kg m^{-3}. Isothermal curves are shown for mixtures of the melt with 5 and 10 wt % (free) water, pure water at 800°C and 1000°C, and the isothermal and adiabatic slopes for perfect gases such as H_2, N_2, O_2, and air.

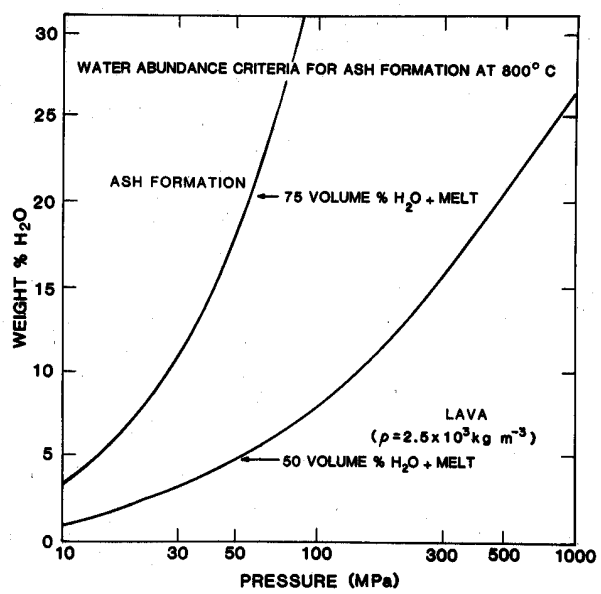

Fig. 4. Plot of weight percent H_2O versus pressure showing the regions of ash formation and lava eruption (see text).

An important aspect of the amount of water (gas) in the melt is that when it occupies about 50% volume fraction, gas becomes the continuous phase and the silicate melt is discontinuous for cubic closest packing of spherical bubbles. *Sparks* [1978] suggests that 75–84% bubble volume fraction approximates the transition of a continuum of melt to particles, which may be thought of as a hexagonal closest packing situation. For simplicity we choose the 50% level as a criterion for ash formation. Table 1 summarizes the specific volume data for water-melt mixes, and Figure 4 is a plot of the weight percent water present (in excess of melt saturation) for ash formation at different pressures. These criteria may be viewed as necessary conditions for an explosive pyroclastic eruption. A smaller weight percent of water results in an extrusion of lava upon bursting. Other factors such as the surface tension and surfactant qualities of the silicate melt may determine the actual amount of gas needed to form ash.

Our model consists of equations representing a magma chamber filled with an isothermal mixture of a melt and water at 800°C and with pressure increasing downward from 100-MPa pressure. The weight percent water present as a separate phase equals or is greater than 8.7% so that ash formation may occur. For simplification, we assume that water as the free phase has separated from the melt and migrated to the chamber top so that the mixture there is nearly all water.

Blast Phase

With failure of the chamber roof, the blast phase commences. High-pressure water at the magma chamber top expands and erupts from the vent. Initially, few melt particles are entrained in the flow, but these increase in abundance as deeper levels of the chamber are tapped. The initial eruption is likened to a one-dimensional shock tube (Figure 2) in which a shock wave moving from the high-pressure region is followed by the high-pressure gas (steam and melt particles). A rarefaction wave recedes into the magma chamber. The resulting vertical flow of gas from the chamber can be determined from the conservation conditions across the shock and rarefaction waves. These conditions are well known and are given here for the one-dimensional case. First, across the shock wave in the atmosphere where Rankine-Hugoniot conditions [*Zel'dovich and Razier*, 1966] hold,

$$\frac{u_3}{c_1} = \frac{(1 - \mu_1)(P_3/P_1)}{[(1 + \mu_1)(P_3/P_1 + \mu_1)]^{1/2}} \quad (1)$$

TABLE 1. Specific Volumes of Water and Magma at 800°C

Pressure, MPa	Specific Volume, $\times 10^{-3}$ m^3 kg^{-1}			Relative vol % Occupied by Melt		wt % Free H_2O Necessary for 50 vol % Ash Formation
		Magma				
	Water	5 wt % H_2O	10 wt % H_2O	5 wt % H_2O	10 wt % H_2O	
100	50.0	2.88	5.40	13	7	0.8
300	14.0	1.08	1.80	35	20	2.8
500	8.50	0.81	1.20	47	30	4.5
1,000	4.20	0.59	0.78	64	46	8.7
3,000	1.95	0.48	0.56	79	64	17.0
5,000	1.70	0.46	0.53	82	68	19.1
10,000	1.00	0.43	0.46	88	78	28.6

TABLE 2. Assumed Initial Values for High-Pressure Steam (Magma) and Atmosphere

Medium	Steam	Atmosphere
T, K	1073	300
c, m s^{-1}	625	340
γ	1.29	1.4
P, MPa	100	0.1
μ	0.126	0.166

and then across the rarefaction wave in the magma assuming isentropic conditions,

$$\frac{u_4}{c_2} = \frac{-2}{(\gamma_2 - 1)}\left[\left(\frac{P_4}{P_2}\right)^{(\gamma_2-1)/2\gamma_2} - 1\right] \quad (2)$$

Variables in the equations are the velocity u, sound speed c, pressure P, the inverse of the adiabatic compression limit $\mu = (\gamma - 1)/(\gamma + 1)$, and isentropic exponent γ which is the ratio of specific heats C_P/C_V. Subscripts (Figure 2) denote (1) atmosphere, (2) magma (steam), (3) compressed atmosphere, and (4) expanded steam. Across the contact surface (the front of ash and steam moving out of the vent) the velocity and pressure are continuous. Therefore $u_3 = u_4$, $P_3 = P_4$, and

$$\frac{c_1}{c_2}\frac{(1-\mu_1)(y-1)}{[(1+\mu_1)(y+\mu_1)]^{1/2}} = \frac{2}{(\gamma_2 - 1)}\left[1 - \left(\frac{P_1}{P_2}\,y\right)^{(\gamma_2-1)/2\gamma_2}\right] \quad (3)$$

where $y = P_3/P_1$ is the shock strength. Equation (3) is transcendental in the shock strength given the initial pressure ratio P_2/P_1 (the pressure in the magma chamber divided by that of the air) and the properties of these two media prior to the eruption, namely, μ, c, and γ.

If the shock strength is known, the jump conditions at the shock are as follows [*Zel'dovich and Razier*, 1966]:

$$u = c_1(1-\mu)(y-1)/[(1+\mu)(y+\mu)]^{1/2} \quad (4)$$

$$U/c_1 = M = [(y+\mu)/(1+\mu)]^{1/2} \quad (5)$$

$$\rho/\rho_1 = (\mu + y)/(1 + \mu y) \quad (6)$$

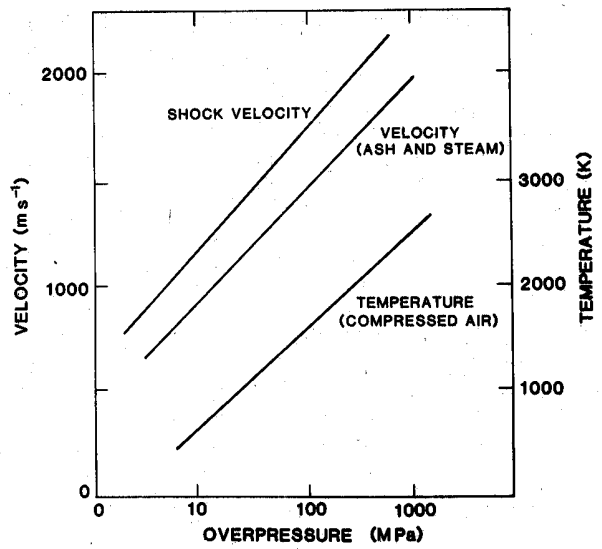

Fig. 6. Initial velocities and temperatures of the shock wave and contact surface (ash behind the shock) for various chamber overpressures. Note that owing to spherical divergence and other dissipative effects, these initial values will quickly decrease with time after the burst.

$$T/T_1 = y(1 + \mu y)/(\mu + y) \quad (7)$$

where u is the velocity of shocked air (i.e., the velocity of erupting material), U is the shock velocity in air, M is the Mach number of the shock, ρ is the density of compressed air, and T is the temperature of compressed air.

Using the initial properties for magma and atmosphere prior to eruption summarized in Table 2, we calculate a shock strength of about 30. Similar solutions for various pressure ratios are shown in Figure 5. For example, an initial overpressure of 500 MPa produces a shock strength of 47, whereas an overpressure of just 10 MPa gives a shock strength of 13. The parameters calculated from equations (4) through (7) for overpressures of 10 to 100 MPa are shown in Figure 6.

The duration of this initial unsteady blast phase of an ash flow eruption is probably a matter of minutes, after which steady flow out of the vent results in a collapsing Plinian column. In reality there is a transition between the blast phase and the subsequent steady flow. As the rarefaction wave moves through the magma chamber, it reflects from surfaces

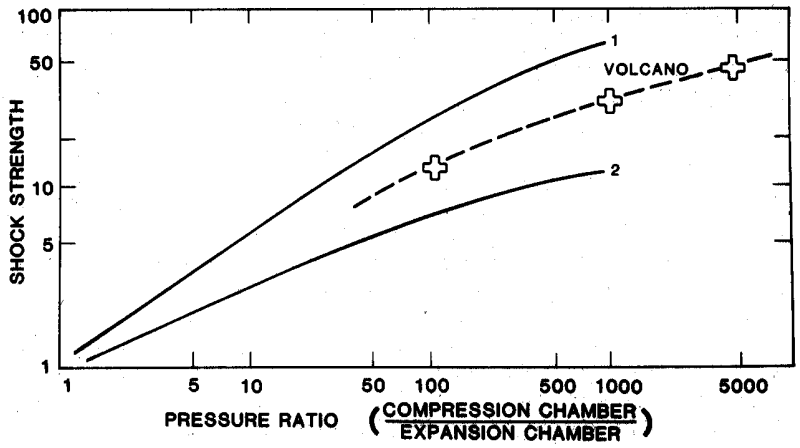

Fig. 5. Shock strength as a function of initial pressure ratio for the volcano model and for two shock tube cases from *Wright* [1967]. Curve 1 represents hydrogen in the compression chamber and air in the expansion chamber, where $\gamma = 1.4$, $\mu_1 = \mu_2 = 1/6$, and $c_2/c_1 = 3.8$. Curve 2 represents air in both chambers, where $\gamma = 1.4$, $\mu_1 = \mu_2 = 1/6$, and $c_2/c_1 = 1.0$.

TABLE 3. Calculated Eruption Velocities Including Frictional Effects

Length, m	Diameter, m	Roughness (E/D)	Friction Factor f	Velocity, m s^{-1}
9000	180	0.01	0.040	501
9000	180	0.05	0.072	383
9000	180	0.10	0.110	314
4000	60	0.01	0.040	439
4000	60	0.05	0.072	334
4000	60	0.10	0.110	272

of density (compressibility) contrast. Above the wave the melt mixture is accelerated upward. Reflections of the rarefaction wave produce compression waves that move up the vent into the atmosphere producing additional rarefaction waves which propagate back into the chamber. Steady flow begins sometime after the reflected rarefaction reaches the vent and becomes well developed only after rarefaction resonances damp out owing to viscous dissipation. The duration of the blast phase roughly equals the effective magma chamber depth divided by the sound speed of the melt mixture (the propagation speed of the rarefaction). The sound speed in the gas-charged melt is unknown and for a two-phase mixture of water and magma may be considerably less than that of either phase [*Soo*, 1967]. However, considering a magma chamber with a pressure of $\simeq 1$ kbar, temperature of $\simeq 800$°C, and water as the continuous phase, a sound speed for supercritical water of $\simeq 625$ m s^{-1} is obtained from calculations by *Kieffer* [1977] and from compressibility and volume data given by *Helgeson and Kirkham* [1974]. Alternatively, the sound speed in the melt mixture at rest may be estimated as for gas dynamics from

$$c = (\gamma P/\rho)^{1/2} \tag{8}$$

For a 100-MPa, 800°C magma chamber of $\rho = 1.3 \times 10^3$ kg m^{-3} (Table 1), $c = 300$ m s^{-1}. Taking the depth to the bottom of a chamber to be 7 km, the blast is therefore >20–40 s. The transition phase might last a slightly longer time because the reflected rarefaction wave propagates more rapidly near the surface owing to upward movement of the magma; however, its velocity probably falls to below 100 m s^{-1} as the wave travels through portions of the chamber where water is vaporizing. *Kieffer* [1981] estimated a sound speed of 105 m s^{-1} for the multiphased magma at Mount St. Helens. Although our shock tube model does not include the effects of magma inhomogeneities, friction along the vent walls, and geometric divergence, it is reasonable to conclude that the combined duration of the blast and transition phase is probably of the order of several minutes or less.

Decompression Phase

Following the unsteady flow phase just described, magma establishes a steady flow from the chamber and vent, forming ash near the top of the vent. The properties of this flow are determined by several factors including the content and distribution of magma volatiles, frictional effects, magma chamber and vent geometry, and pressure history within the chamber.

The problem of volatile content and distribution within the magma is simplified by assuming isobaric conditions and 50 volume percent criteria for ash formation in the upper part of the magma chamber. We take the magma chamber geometry (i.e., depth of chamber top of $\simeq 3$ km, 22-km diameter hemispherical chamber) from *Smith* [1979], and we take the pressure history of the chamber to be constant. This consideration is based upon observations that the roof of the magma chamber often collapses during eruption, maintaining lithostatic pressure on the magma and offsetting the magma volume decrease within the chamber. Our model is therefore one in which the chamber roof collapse acts as a piston to maintain constant pressure in the melt.

The earlier assumption of ring dike vent geometry can also be simplified. The effective diameter D_h of a rectangular vent modeled as a cylinder is about 4 times its hydraulic radius R_h which is defined by

$$D_h = 4R_h = 4A/P_w \tag{9}$$

where A is the area of the vent and P_w is its wetted perimeter. For a linear or ring dike vent 1000 m long and 100 m wide, an equivalent model is a circular vent 180 m in diameter. A linear vent 4 km longer would change the hydraulic diameter only slightly to $D_h = 196$ m.

After a steady flow of ash and steam is established in the vent from initial conditions nearly the same as considered earlier (Table 2), simple estimates of the flow conditions can be made assuming an ideal case in which the vent width is small in comparison with that of the underlying chamber. This geometry is comparable to a convergent duct where isentropic flow is choked and material vents with the sound velocity and at a critical pressure derived by *Miles* [1950]:

$$P^* = P_2\left(\frac{2}{\gamma+1}\right)^{\gamma/(\gamma-1)} \tag{10}$$

$$u^* = c^* = \left(\frac{2}{\gamma+1}\right)^{1/2} c_2 \tag{11}$$

$$\rho^* = \rho_2\left(\frac{2}{\gamma+1}\right)^{1/(\gamma-1)} \tag{12}$$

For $P_2 = 100$ MPa, $\gamma = 1.29$, $c_2 = 625$ m s^{-1}, and $\rho_2 = (\gamma P_2)/C_2{}^2 \simeq 0.33 \times 10^3$ kg m^{-3}, the jet density is $\rho^* \simeq 0.2 \times 10^3$ kg m^{-3}, the velocity is $u^* = 584$ m s^{-1}, and the pressure is $P^* = 548$ MPa. These equations may not apply in cases where erosion of vent walls and pyroclast deposition around the vent form an expanding nozzle with dimensions appropriate for Venturi-like flow [*Wilson et al.*, 1980].

The flow of ash and steam is not entirely free of boundary friction owing to the roughness of the vent. In the case of a dike with a hydraulic diameter of 180 m, reasonable values of relative roughness (E/D, where E is a size characteristic of the wall roughness and D is a characteristic dimension such as diameter) may range from 0.1 to as low as 0.01 for well-developed vents [*McGetchin and Ullrich*, 1973]. We use *Miles'* [1950] approximate equation for steady compressible flow with friction to evaluate the reduced velocity $\tilde{u}^*$ where f is the friction factor for a given surface roughness and L/D is the length and diameter of the vent. The velocity is

$$\tilde{u}^* \simeq c_0\left\{\frac{[2/(\gamma-1)][1-(P_4/P_2)^{(\gamma-1)\gamma}]^{1/2}}{L + 4fL/D}\right\} \tag{13}$$

The velocities of flow including friction are shown in Table 3. Predicted eruption velocities with frictional effects range from 270 to 500 m s^{-1} and are substantially less than an ideal isentropic model suggests.

TWO-DIMENSIONAL EULERIAN COMPUTER SIMULATION

A numerical solution of two-phase flow hydrodynamic equations gives the variation in time and space of gas temperature and pressure, ash particle velocity, bulk density, and flow field geometry. These equations can therefore be used to produce a more detailed model of Plinian eruptions, and the results can be compared with the simple estimates made above. The implicit continuous-field Eulerian (ICE) method [*Harlow and Amsden*, 1971] is a finite difference method for numerical solution of multidimensional flows in which the Mach number ranges from subsonic to supersonic values. A variation of ICE known as the implicit multifield (IMF) method [*Harlow and Amsden*, 1975] was developed for two-phase flows containing a mixture of liquid and gas bubbles or a gas containing droplets or particles. A computer program named KACHINA [*Amsden and Harlow*, 1974] implements the IMF method in two-dimensional cyclindrical geometry and has been applied to Plinian eruptions. KACHINA considers both compressible gas and incompressible (ash) fluid phases and couples them by means of two-phase flow hydrodynamic equations. Two fields (phases) are considered: the incompressible country rock and compressible atmosphere. The magma chamber region is a partly compressible mixture of these two fields. The coupled fields are represented on a two-dimensional axisymmetric grid of fixed constant-dimension Eulerian cells through which the fluid mixture moves. Momentum exchange coupling is achieved by a drag function which depends upon the particle size, fluid porosity, and the Reynolds number [*Amsden and Harlow*, 1974]. The numerical solution involves an iterative sequence of finite difference computation cycles employing donor cell differencing. The time implicit difference method circumvents the need for an explicit artificial viscosity term to achieve stability [*Hirt*, 1968], but the time step used must obey the usual Courant-Fredricks-Levy condition when shocks are present in the calculation.

Model Parameters

The initial boundary conditions model (1) a two-dimensional axisymmetric vent of 5.0-km diameter over a partly compressible magma chamber with a rigid reflective base at 7.5 km below the ground surface, (2) incompressible country rock surrounding the vent, and (3) a compressible atmosphere extending 17.5 km above and 10 km in radius from the vent. Table 4 summarizes the physical parameters of the computer model illustrated in Figure 7. These parameters may be compared with those used in the shock tube model (Table 2). The country rock is at 165 K, of uniform density at 2.7×10^3 kg m^{-3}, and is at a surface pressure P of 0.07 MPa which increases with depth. The model includes no provisions for material strength, and all materials are mathematically treated as fluids.

TABLE 4. KACHINA: Code Model Parameters

Field Parameter	Model
	Atmosphere
Compressible medium	voided space, H_2O vapor as ideal gas
T_1, K	274
c_1, m s^{-1}	340
γ_1	1.4
P_1, MPa	0.08 (decreasing with height)
μ_1	0.166
	Magma
Partly compressible medium	50% solid 1-mm particles, $p = 2.7$ 50% steam (ideal gas) in voids
Vent size	5000-m vent width
T_2, K	1070
c_2, m s^{-1}	calculated: $c = (\gamma P/\rho)^{1/2}$
γ_2	1.29
P_2, MPa	90 (increasing with depth)
μ_2	0.126

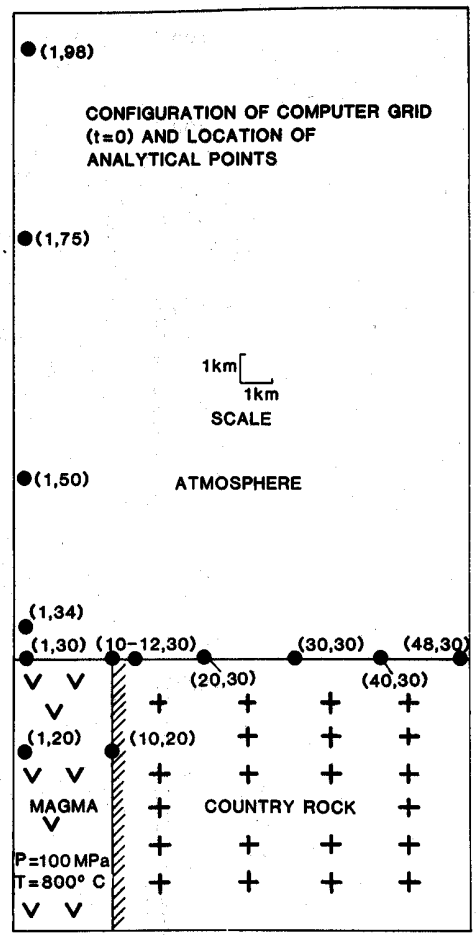

Fig. 7. KACHINA mesh setup for the volcano simulation. The magma chamber is shown axisymmetrically in the lower left. It contains a partly compressible fluid mixture of water (steam) and particles. The country rock is incompressible fluid and the atmosphere is an ideal gas. Points with coordinates show grid locations (gauge stations) where various parameters were analyzed with time.

Results

In order to analyze the results of the numerical calculation we constructed profiles of gas velocity, temperature, and pressure as a function of time at various positions on the vertical axis and at points spaced radially outward at the ground level. Plots of these variables at selected mesh locations are shown in Figures 8 and 9. The arrival times of the shock wave are shown by the first peaks on the plots, and subsequent peaks result from reflections of the rarefaction wave. Because hot ash particles move out of the vent directly behind the shock front, gas pressure, velocity, and temperature continue to rise after passage of the shock front. Estimation of the shock front location requires analysis of calculated gas density increases.

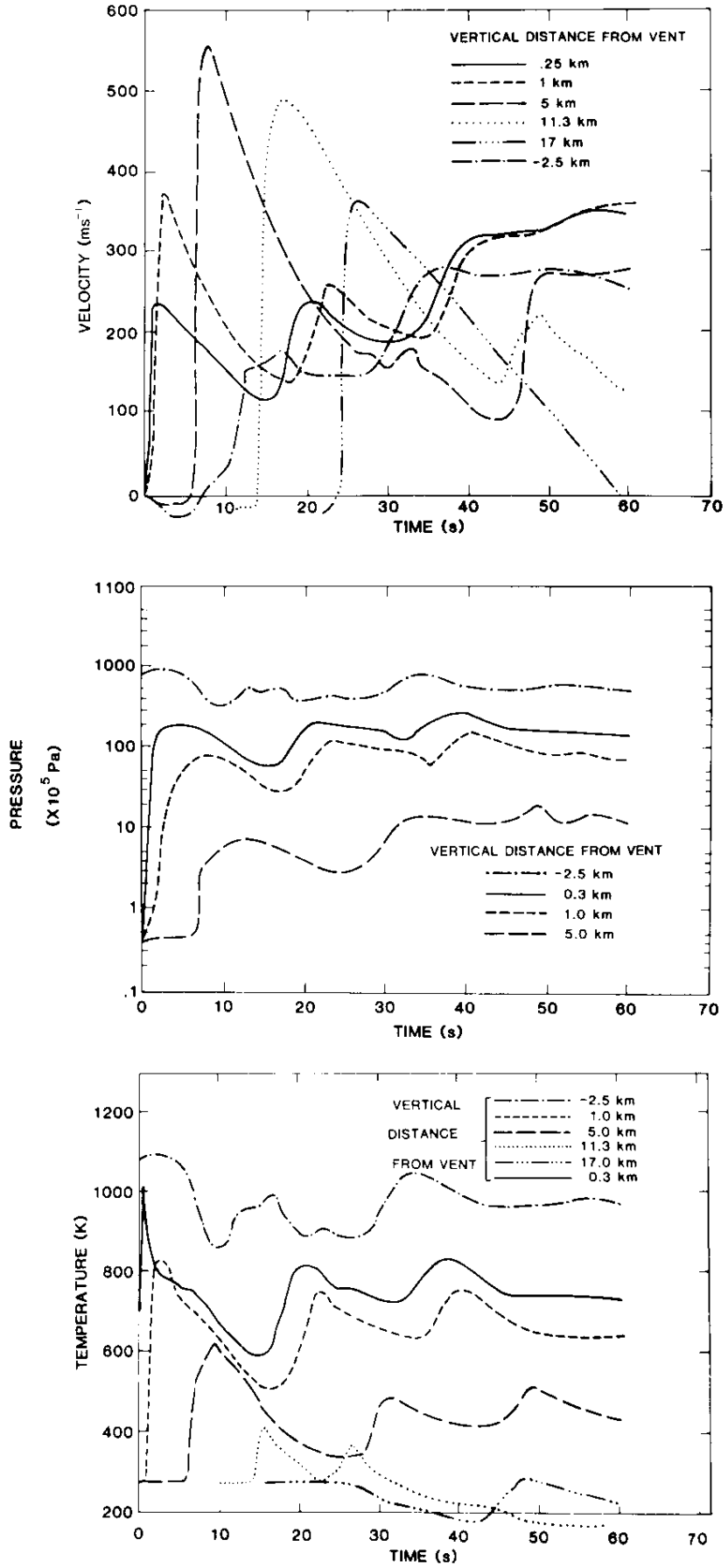

Fig. 8. Plots of vertical axis gas velocities, temperatures, and pressures versus time at different grid points. The first peaks show the arrival of the shock wave with later peaks due to compression waves generated by reflected rarefactions in the vent. Temperaures and pressures are also affected by arrival of the ash contact shortly after the shock wave.

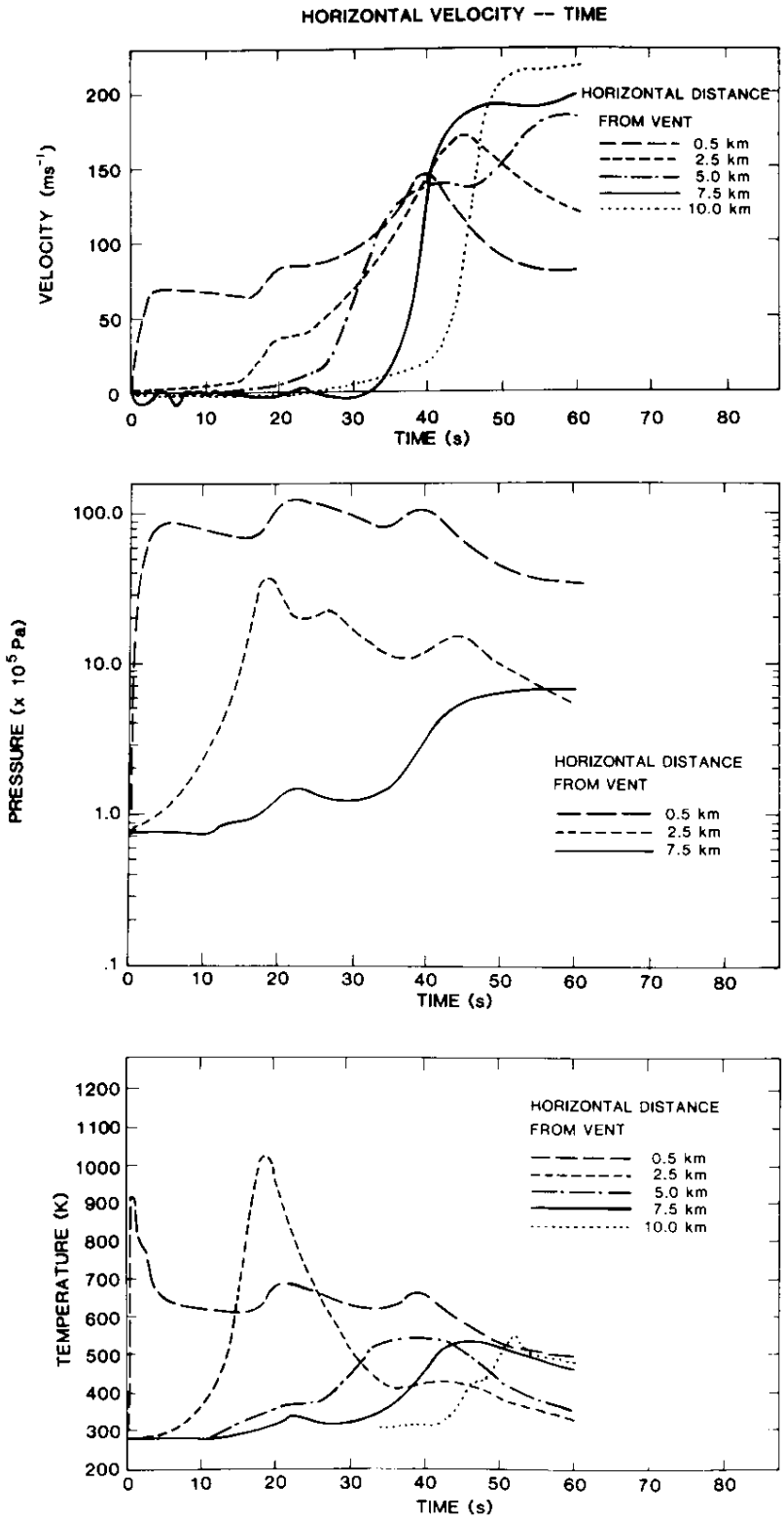

Fig. 9. Plots of horizontal axis (ground level) velocities, temperatures, and pressures versus time. Values are somewhat less than along the vertical axis because the shock diffracts around the vent rim from its initial, vertically propagating configuration. Note that arrival of the ash contact after the shock limits the decrease in values after shock passage.

The shock front is found to be slightly ahead of peak pressures and temperatures but is not well resolved.

Blast phase. The peaks in Figure 8 show that the shock accelerates from 340 m s^{-1} at 1 km above the surface to over 750 m s^{-1} at 10-km altitude. This increase is due to the decrease with height of pressure and density in the atmosphere. Maximum atmospheric gas velocities which occur about 5 km above the vent are $\simeq 550$ m s^{-1}. Atmospheric pressure and temperature increases behind the shock are 1–10 MPa and 1000 K, respectively, at 1 km above the vent. These values

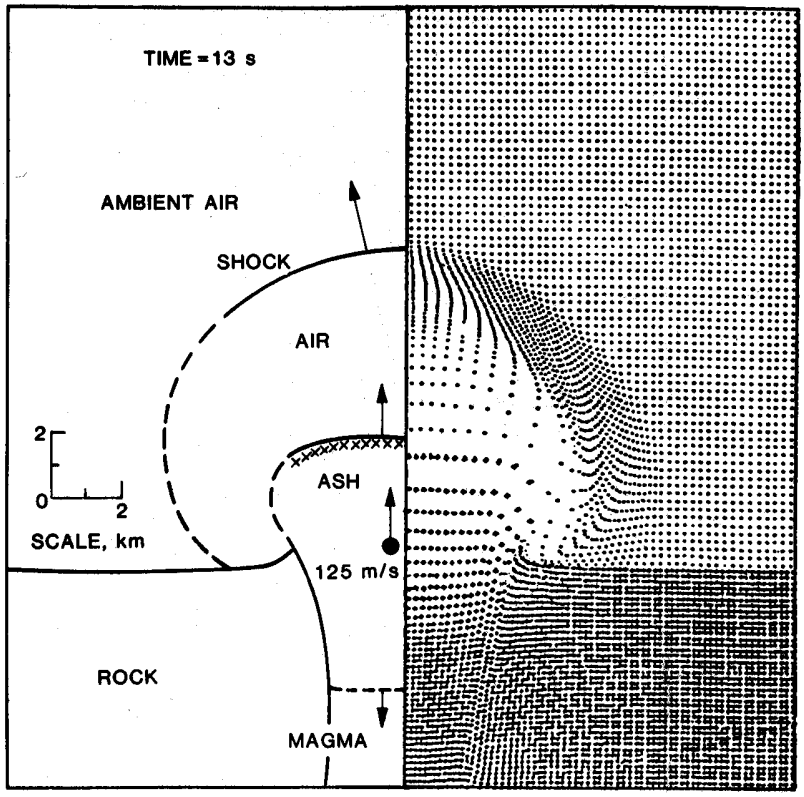

Fig. 10. Schematic representation and KACHINA marker particle plots at 13 s showing the shock wave, ash contact, and rarefaction wave in the vent.

decrease quickly with increasing altitude owing to divergence of the blast wave.

Horizontal axis plots (Figure 9) are of great interest to predict the volcanic hazard due to blast phenomena. Plots of temperature and pressure histories at various radii from the vent show the dissipation of blast effects with increasing distance. The shock wave initially moves upward and also diffracts around the vent rim in a manner analogous to Prandtl-Meyer expansion [*Shapiro*, 1953]. This effect propagates a weak shock along the ground at about sound speed. The effects of this compression wave can be estimated from Figure 9. At 2.5-km radius from the vent the atmosphere is heated to 450–900 K and compressed to 0.2–2 MPa. These values decrease to 450–550 K and 0.15–0.7 MPa at a 10-km radius from the vent. Velocities produced by the wave may exceed 200 m s^{-1} at 10-km radius. The shock produces wind velocities that increase with distance. The duration of the blast phase can be estimated from the arrival time of the first and subsequent peaks on plots at −2.5-km depth in Figure 8. These peaks are due to rarefactions and indicate a duration of 20 to 40 s which corresponds to a magma chamber sound velocity of between 250 and 750 m s^{-1}. The transition phase after the blast appears to last nearly a minute before steady flow of ash starts.

Decompression phase. Trajectories of massless marker particles (Figures 10 and 11) provide a visualization of the eruption at several times. The ejected ash expands behind the shock wave forming a hemispherical contact surface. The high-temperature ash front velocities are near 250 m s^{-1} upward and 125 m s^{-1} horizontal for the first 30 s. Horizontal speeds accelerate to nearly 340 m s^{-1} from 30 to 60 s. The reason for the acceleration after 30 s appears to be due to the extra push given by the reflected rarefaction wave which emerges from the vent about 20 s behind the ash front and catches it after 40 s.

Discussion of Computer Model

Figure 12 is a distance versus time plot for results from our computer model. When compared with that of an ideal one-dimensional shock (see Figure 2), the distance-time plot reveals the simple shock tube model to be a reasonable approximation. The temperature and pressure profiles in Figure 13 may also be compared with those predicted by shock tube theory [*Wright*, 1967].

To assess the precision with which the KACHINA code calculates a shock wave, we examine the data in Figure 13. The calculated pressure jump implies a shock strength of 20 to 30 (equation (3)) corresponding to a temperature rise to 800 K, which compares well with the numerical result. Both temperature and pressure continue to rise behind the shock owing to arrival of the ash front; however, the inflection of the temperature profile reasonably locates the shock front which is smeared by numerical diffusion.

Although there are definite limitations of the computational method due to use of donor cell differencing and approximations made in the momentum coupling of the magma with country rock and atmosphere, some qualitative aspects of particle path plots (Figure 11) are of interest. An expanding shock diffracts around the vent rim after the first several seconds forming a hemispherical shock front. The hydrodynamic coupling with the ground surface (treated as a dense fluid) is evident in horizontal velocity plots (Figure 9) where negative (toward the vent) velocities of about 10 m s^{-1} occur at $\simeq$7.5-km radius. One likely explanation of this phenomenon is an "afterwind" convective inflow similar to that seen in nuclear detonation [*Glasstone and Dolan*, 1977]. At later

times, particle path plots show an uplift and curling outward of the vent rim as ash accelerates past. By 30 s the vent flares outward considerably owing to momentum transfer from the ash to the vent walls. A high concentration of ash particles flows along the ground surface. A qualitative interpretation of the transient inflow velocities and vent rim phenomena is that a ground surge forms. The fact that it is only well developed after 30 to 40 s is partly due to the effects of the reflected rarefaction wave which exits from the vent as a compression wave at 20 s and catches the incipient surge at 30 s. The added impulse of this compression wave accelerates the surge to near sonic velocities.

Contour plots of gas volume fraction (Figure 14) show that ash particles erupt from the vent and move along the ground horizontally as is expected for a pyroclastic flow. The high-density ash cloud rises $\simeq$2.5 km above the vent and spreads radially outward along the ground surface in a flow several hundred meters thick. These plots of gas volume fraction at 10 and 60 s can be compared with those of vapor isotherms at 10 and 30 s in Figure 15. The isotherms define the passage of the shock front which is predominantly in the vertical direction. The gas volume fraction plots, however, do not show the vertical eruption plume that forms because the plotting limit is less than that typical of an eurption plume (gas volume fraction 0.99999 corresponds to $\simeq 1.91 \times 10^4$ solid particles of 1-mm diameter per cubic meter).

Another aspect of the computer model that deserves attention is the pressure and wave velocity forms (gauge signals),

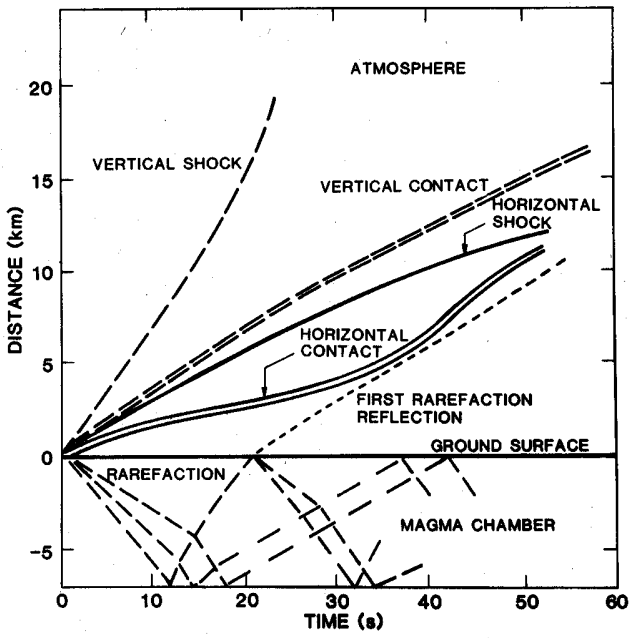

Fig. 12. Distance-time plot for the computer model shows development of shock tube physics as illustrated by movement of the shock wave, contact surface, and rarefaction wave. The horizontal and vertical components of the shock and contact are plotted separately. The horizontal movement has been decreased because of apparent ground coupling. Note that the emanation from the magma chamber of the reflected rarefaction corresponds in time to acceleration of the horizontal contact line.

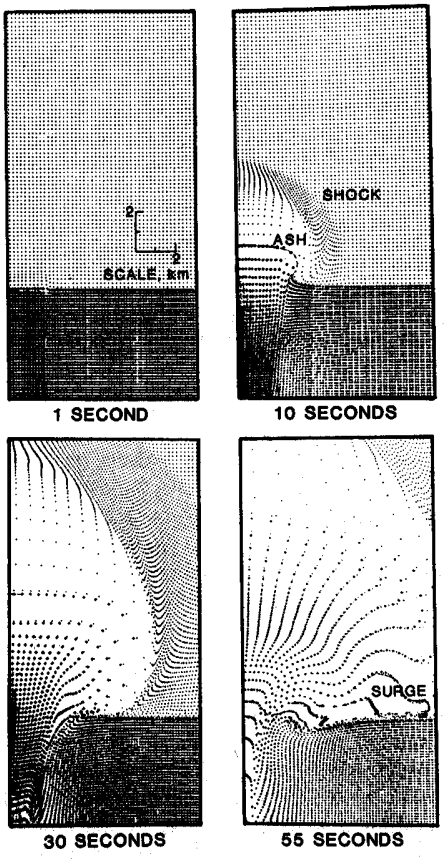

Fig. 11. Marker particle plots at 1, 10, 30, and 55 s after eruption. These plots show the initial planar shock developing into a hemispherical shock, overturn of the vent rim, movement of the ash particles behind the shock, and development of a ground surge at late times.

especially at points along the vertical axis (Figure 8). Reflections of the initial rarefaction develop a resonance in the vent which is apparent as velocity pulses in later times. This acoustic echoing develops a pulsed propagation of erupted ash particles so that they move in a fluctuating flow with a period dependent upon the vent geometry, in this case about 20 s. Although Figure 8 shows the effect of rarefaction waves reflected within the vent, rarefactions associated with the vent rim (rarefaction fan, *Kieffer* [1981]) may reflect from the flow boundary (the ground surface of this model) as compression waves that coalesce and form weak shocks. Such details are beyond the resolution of our calculation, but these are also likely contributors to the surge and the formation of the vent rim.

A most interesting albeit obvious result is vertical acceleration of the shock into the atmosphere. The density decreases exponentially upward in the atmosphere, as does the pressure and density behind the shock. The KACHINA calculations show that at 17.5 km above the vent, the scale height of exponential decrease in density behind the shock is greater than that in the earth's atmosphere. Consequently, the heated air behond the shock will be out of density equilibrium with the ambient atmosphere and will accelerate down the atmospheric pressure gradient. Ash carried behind the shock will therefore attain great altitudes, piercing the tropopause and achieving wide (perhaps global) distribution before falling back to earth.

IMPLICATIONS FOR LARGE EXPLOSIVE ERUPTIONS

To demonstrate the utility of the simple shock tube model, we present an application to the eruption of the Bandelier Tuff from the Valles caldera around 1 m.y. ago. First, some background on the geologic constraints will be discussed, and then results of simple one-dimensional calculations are given.

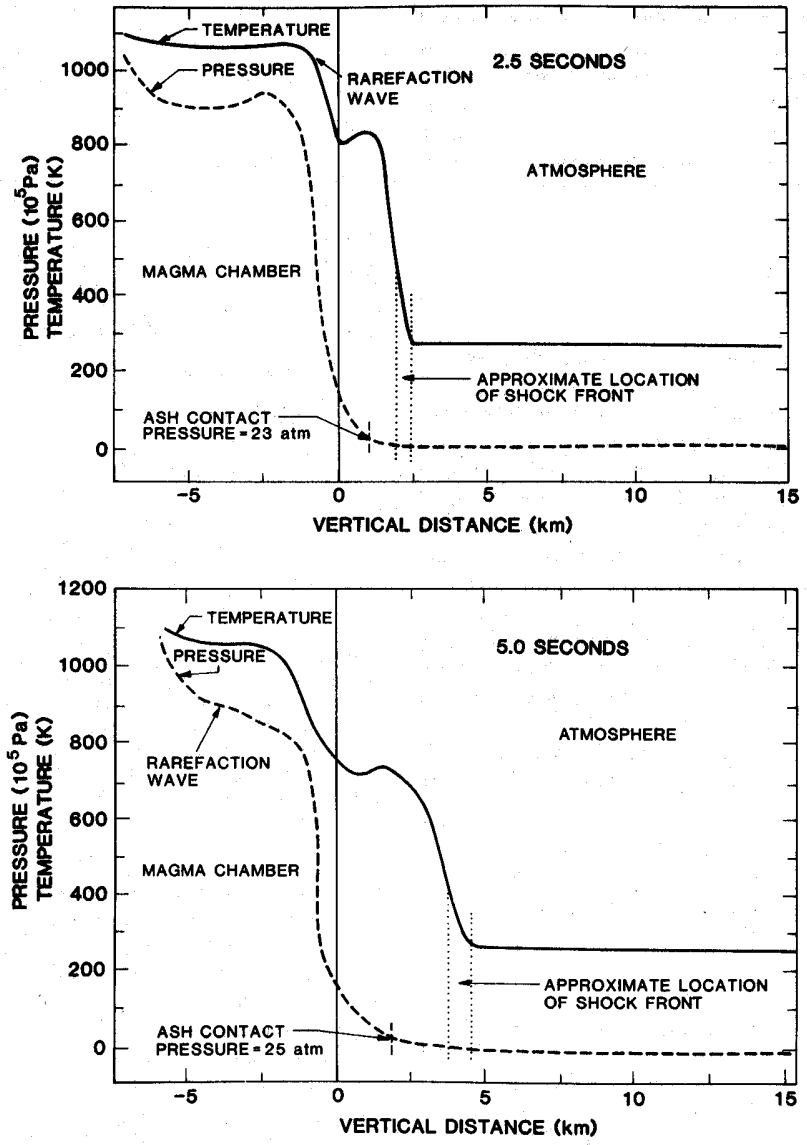

Fig. 13. Profiles of pressure and temperature versus distance at 2.5 and 5.0 s after burst. The ash contact is within one grid zone of the shock at early times. Location of the ash contact by Lagrangian marker particle path plots shows the approximate pressure and temperature effects due to the shock alone.

Valles Caldera Model

Smith [1960] and *Smith and Bailey* [1961, 1968] produced a detailed model for the evolution of calderas that erupt with large-volume ashfall and pyroclastic flows. Their work is based in part upon a long and very extensive mapping program focused on the Valles caldera, in the Jemez Mountains of New Mexico. The history of the Jemez volcanic field has recently been summarized by *Gardner* [1982, 1983]. The important geologic aspects of the Valles caldera formation are summarized here.

The catastrophic eruption of the Tshirege member of the Bandelier Tuff was probably accompanied by collapse of the magma chamber roof into the evacuated part of the chamber. This conclusion is drawn from field evidence [*Dondanville*, 1978] which shows that a greater thickness of tuff accumulated within the caldera than on its flanks. Accordingly, a topographic low area must have formed above the chamber during eruption. The step-faulted nature of the Precambrian basement under the caldera [*Segar*, 1974; *Goff*, 1983] suggests that the roof remained a semicoherent mass during the Plinian eruption and that venting occurred along the margins of the caldera which are steeply dipping ring fault systems.

Both the Yellowstone Park caldera [*Christiansen and Blank*, 1972] and Long Valley caldera [*Bailey et al.*, 1976] show caldera formation sequences similar to that of the Valles. A simple interpretation of the eruption sequence follows. Ash composition and structural considerations indicate that prior to the caldera-forming eruption, a large silicic to intermediate composition magma chamber forms in the upper crust at depths of 3 to 10 km. Cooling and crystallization within this magma chamber results in chemical zonation. Thus magma becomes progressively more silicic toward its top and more mafic near its base [*Hildreth*, 1979]. One result of chemical zonation within a magma chamber is the concentration of volatiles (dominantly H_2O, which may be of meteoric origin [*Sheridan and Wohletz*, 1983]) near the top. When the roof of the chamber fails, rapid decompression of high-temperature volatiles drives an explosive eruption. Part of the eruption

energy is manifested in fragmentation of the magma to form ash and pumice. The eruption proceeds until volatiles become depleted in the magma and the magma freezes in response. Late stage eruption of lava evidently results from the hydrostatic equilibration of incompressible lava with relatively denser country rock [*Fink*, 1983].

Smith et al. [1970] show the Valles magma chamber top resided 3 to 4 km below the surface, which suggests that the chamber pressure was at least 100 MPa. Additionally, *Smith* [1979] has shown a positive correlation of ash flow volumes with caldera area. Accordingly, a first-order approximation to the magma chamber volume is made by assuming that the chamber volume is 1 order of magnitude greater than that of the caldera-forming eruption products [*Smith and Shaw*, 1975]. Using this approximation, *Smith* [1979] calculated the depth of drawdown in a hemispherical magma chamber during caldera-forming eruptions assuming a hemisphere diameter equal to that of the caldera itself. The assumed diameter fits various geologic observations of large-volume eruptions. Thus the 22-km-diameter Valles caldera formed above a magma chamber of about 3×10^3 km^3 volume. The 300 km^3 of magma which erupted during the collapse associated with the Tshirege member of the Bandelier Tuff represents a nearly 10% drawdown of the magma chamber. This drawdown is equivalent to a 4-km vertical depth in a spherical chamber top and would have allowed $\simeq$1-km vertical collapse of the 22-km-diameter caldera area. This estimate is in agreement with the topography and geophysical models [*Segar*, 1974] of the present-day caldera fill.

These physical constraints, the magma properties summarized in Table 2, and a depth to the top of the chamber of 3 km with approximately 4 km to the bottom of the erupted portion of the chamber lead us to derive the model which follows. Only the assumption of vent size remains to be constrained by field studies. As discussed earlier, if a linear vent system situated along ring fractures is realistic, then a change in the length of such a vent affects the hydraulic radius very little. Thus we assume a 1- to 5-km long by 0.1-km wide vent.

The shock tube model of the Valles caldera predicts that the blast produced a shock wave which traveled at 1740 m s^{-1}, heated and compressed the air behind it to 1550°C and 3 MPa, respectively, but gradually dissipated owing to spherical divergence. Initially, ash and country rock moved from the vent at nearly 1500 m s^{-1} during the first few tens of seconds until a stabilized ash and steam plume formed. In the plume stage the velocity in the vent decreased to around 300 to 500 m s^{-1} and column collapse began. For an assumed vent area of 1 km $\times$ 0.1 km, the predicted eruption rate was 1.2×10^{10} kg s^{-1} which may be compared with *Walker*'s [1980] data for maximum limits. Each unit of the Bandelier Tuff is about 300 km^3 [*Smith*, 1979] at magma density or, at emplacement density of $\simeq 1 \times 10^3$ kg m^{-3}, 750 km^3. This eruption rate gives an ash flow emplacement time of 6.3×10^4 s ($\simeq$18 hours). We conservatively conclude that ash flow eruption of each Bandelier member occurred over a span of 1 to several days. The calculated velocity values compare well with those of *Wilson et al.* [1980] as do the correlations of vent diameter versus mass flux (180 m for 10^{10} kg s^{-1}). The stabilized jet velocities also compare well with observations of eruptive columns [*Lirer et al.*, 1973; *Minakami*, 1942; *Walker and Croasdale*, 1971; *Self et al.*, 1979] in the range of 200 to 600 m s^{-1}. Furthermore, our calculations require at least 8.7 wt % water in the top of the Valles magma chamber. This water abundance is similar to those calculations of *Wilson et al.* [1980] that compare ash flux to water content, vent radius, and pressure. When our values are applied to the plots of *Sparks et al.* [1978] and *Wilson et al.* [1980], they predict a Bandelier Plinian column height of >55 km, in agreement with *Self and Wright* [1981]. The collapse of the gravitationally unstable portion of the column would have occurred over a height of approximately 5–10 km above the vent.

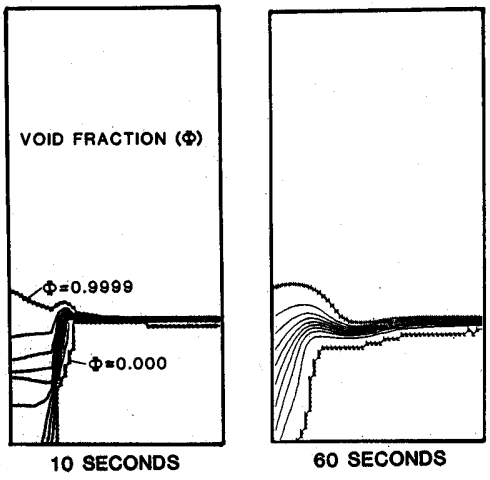

Fig. 14. Contour plots of gas volume fraction at 10 and 60 s. Minimum (L = 0.0) and maximum (H = 0.99999) contours show the densest part of the eruption column and its horizontal outflow.

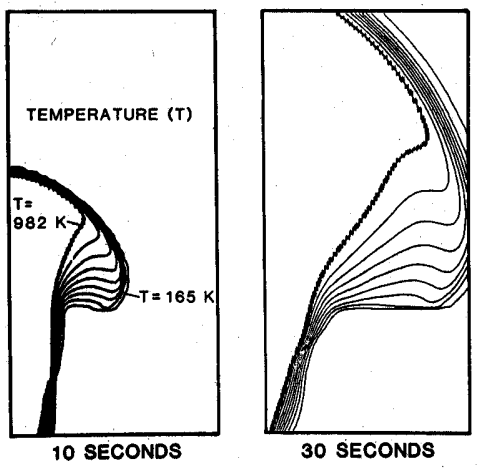

Fig. 15. Contour plots of particle temperature at 10 and 30 s. Minimum (L = 164 K) and maximum (H = 982 K) contours show the development of the shock front which is located where the temperature gradient is steepest. The weak horizontal development of the shock is well illustrated by the distance-time plot in Figure 12.

Discussion

True shock tube–like conditions are unlikely in nature because the initial rupture of a volcanic edifice may never occur in the catastrophic manner of a shock tube diaphragm. In any case the ash loading invalidates the strict application of gas dynamic shock tube theory. Hence additional explanation is required to fit a shock tube blast model to observed ash flow stratigraphy [*Sparks*, 1976]. The occurrence of ground surge deposits above pumice fall deposits is a very common sequence present at the base of large caldera-related ash flows and is clearly a two-dimensional effect. This stratigraphy indi-

TABLE 5. Comparison of Shock Tube and Computer Models With Observed Blast Eruption Parameters

Parameter	Shock Tube	KACHINA*	Observed
Shock velocity, m s^{-1}	1740	600–800 (340)	1600† 600‡ 325§
Shock strength	30	20–30 (1.15–10.0)	1.003‡ 1.60§
Shock compression temperature increase, °C	1525	700 (100–400)	20§
Rarefaction velocity, m s^{-1}	625	250–750	105§
Length of blast phase(s)	20–60	20–40	10–20§
Ash velocity, m s^{-1}	300–500	200–350	1100† 400‡ 325§

*Horizontal direction values shown in parentheses.

†*Livshits and Bolkhoritinov* [1977]: cinder cone eruption in Kamchatka, 1975.

‡*Nairn* [1976]: explosive eruption of Ngauruhoe, 1975. Barograph record of shock strength at location ≃8.6 km from the vent.

§*Kieffer* [1981]: May 18, 1980, Mount St. Helens blast.

cates that Plinian eruption has been active prior to the blast phase. The model envisioned here requires blast to be generated by a catastrophic failure of the vent which sends acoustic waves into the chamber and allows rapid decompression. A catastrophic failure of the vent, or vent widening, may not occur at the initiation of eruptive activity. It can occur after several hours or days of pumice eruption through a small cracklike vent as is indicated by the typical stratigraphic succession from pumice fall through surge to pyroclastic flow. Only after that length of time has there normally been enough thermal or mechanical energy transferred to the vent walls to allow massive, catastrophic failure of the vent. The energy transfer to vent walls is apparent in our two-dimensional numerical results and may be significant to formation of the Plinian eruption column. The actual large-scale failure of vent walls causing vent widening may be due to hydrofracture of water-saturated country rock surrounding the vent [*Knapp and Knight*, 1977]. Thus shocks can be initiated by catastrophic vent widening at the beginning or during eruptive activity. Furthermore, atmospheric shock waves related to volcanic activity have been described at Hekla [*Thorarinsson and Sigvaldason*, 1972] and Mount Pelée [*Perret*, 1935] as flashing arcs and as condensation fronts at Ngauruhoe [*Nairn*, 1976] and at Tolbatchik, Kamchatka [*Livshits and Bolkhoritinov*, 1977].

The shock tube interpretation is especially useful for describing the effects of individual explosions occurring during eruptive sequences (e.g., Krakatoa), a phenomenon that is difficult to assess from interpretation of stratigraphy. The results of the computer simulation of the blast phase show a strong resemblance to shock tube phenomena. Hence the computer modeling method can be combined with geologic constraints to develop detailed scenarios for eruption effects for specific volcanoes. The calculation of actual eruption phenomena requires a detailed knowledge of stratigraphy (see, for example, *Sparks* [1976]), and results are meaningful only when interpreted in that light, which illuminates the limitations and strengths of the model. The use of numerical models to predict volcanic hazards is of prime interest. Further applications to formation of geothermal reservoirs and pyroclastic deposits are topics for future consideration.

Assessment of Model Results

Since no truly large Plinian eruptions associated with caldera collapse of the Valles type have been observed, comparison with observed eruptions is limited to scaled effects. The first question to ask is how similar to a shock tube is the opening blast of a large eruption. Since explosion data for very large caldera-forming eruptions is lacking, this question is best answered by evaluating the two-dimensional computer model of eruption physics (our best estimate of data) in terms of the one-dimensional shock tube theory. Table 5 compares the numerical model results with the gas dynamic theory and observational data. Essentially, we find that KACHINA code analysis of volcanic eruptions shows a strong resemblance to shock tube phenomena when we take into account the divergence and dissipative effects not included in the simple one-dimensional shock theory. Shock strength, rarefaction velocity, and blast duration are the same for both models. The smaller values of shock velocity, temperature increase, and ash velocity computed by KACHINA result from numerical diffusion, resolution, and two-dimensional effects which all tend to smooth peak values over a range of zones. Dissipative parameters such as drag, viscosity, gravity, and particle-atmosphere heat exchange can be treated by KACHINA and also introduce departures from the velocities, temperatures, and pressures calculated from simple equations. In this way the computer solution generates values that can be used to evaluate the importance of the physical processes.

The observations in Table 5 are of much smaller eruptions than the one modeled; so only a superficial comparison can be made regarding magnitude. The modeled eruption involves an erupted volume of the order 100 km^3, whereas those of observed eruptions are 0.1 to 1.0 km^3. Observed shock and ash velocities vary greatly, but these values bracket those computed for the models and appear to be less sensitive than thermodynamic quantities to eruption magnitude. The rarefaction velocity and burst phase duration depend upon reservoir size and the value of sound speed in the reservoir as mentioned earlier. Although estimation of eruption parameters at Mount St. Helens [*Kieffer*, 1981] was carefully made and is likely to be accurate, the similar length of the burst phase for that eruption and the Valles model is probably fortuitous because of the dependence upon estimates of the rarefaction velocity.

Volcanic Hazards Associated With Blast

Volcanic hazard analysis is a field rapidly expanding in two areas: geophysical and statistical prediction, and damage analysis. Blast effects from the 1980 Mount St. Helens eruption appear to have been the primary destructive and loss of life event, even though no well-developed shock wave was documented. This conclusion holds for near-vent localities and does not take into consideration subsequent mud slides and flows and far-field atmospheric ash [*Moore and Sisson*, 1981; *Hoblitt et al.*, 1981; *Kieffer*, 1981]. Thus in a volcanic hazard analysis an eruption involves both shock wave effects and collateral damage due to particle transport in the pryoclastic surge and landslide phenomena. Because of irregularities in vent geometry, initial unsteady ash flow, vapor explosion due to rapid decompression of superheated or supercritical water at (or perhaps downslope from) the vent, a horizontally accelerating, surging flow may develop. Surges are generally considered to be of low initial particle concentration, and when

coupled with rapidly expanding water vapor, they contribute to blast phenomena.

Kieffer [1981], *Malin and Sheridan* [1982], and *Sheridan* [1979] consider a simplified model of the near-vent effects of a pyroclastic surge associated with a blast. Both consider the accelerating motion of the blast by the expression

$$a_x = g(\sin \beta - \mu \cos \beta) \tag{14}$$

where a_x is the acceleration of the surge, β is the slope of the surface, g is the gravitational acceleration, and θ is a measure of frictional effects. *Kieffer* [1981] designates θ as the coefficient of friction ($\theta = 0.12$), and *Malin and Sheridan* [1982] in their heuristic model take θ as the slope tangent of the flow energy line (the Heim constant, an empirical relationship between observed runout distances and flow mobility, grain frictional effects, and the potential flow surface [*Hsü*, 1975]). Only the initial velocity is needed to predict runout distances and times if one neglects local topographic irregularities. *Kieffer* [1981] estimated the initial steady flow velocity u_i as 104 m s^{-1} from

$$u_i = \left[\frac{2}{\gamma_2 + 1}\right]^{1/2} c_2 \tag{15}$$

where γ_2 and c_2 are the adiabatic exponent and sound speed estimated for the magma reservoir contents. Alternatively, *Malin and Sheridan* [1982] estimate initial velocity by

$$u_i = (2g\Delta h)^{1/2} \tag{16}$$

where Δh is height above the vent from which the ash particles collapse to form the surge (this model assumes that an eruptive column collapses to form a surge).

When the variation of slope with distance from the vent is considered, the above models predict lateral limits of blast or surge damage. Returning to the Valles model, the horizontal velocity of ash calculated by KACHINA ranges from about 125 m s^{-1} (Figure 12) for the first 10 s and accelerates to 330 m s^{-1} after 48 s of runout. The initial acceleration of the surge may form a compression wave that reinforces the leading shock front and could possibly generate a subsequent shock at greater distance from the vent [see *Kieffer*, 1981]. Given a pre-Bandelier slope of $\simeq 2°$ (from present Bandelier plateau) and assuming a runout distance of 40 km and a collapse height of 5 km above the vent, the slope of the energy line was 9°. This gives a Heim constant, $\theta = 0.16$. Thus the initial pyroclastic blast decelerated (equation (14)) by -1.2 m s^{-2} from a velocity of 330 m s^{-1} after traveling 10 km in 48 s (Figure 12). After an additional 275 s (30 km of travel) the surge dissipated (Figure 16). The horizontal shock was nearly acoustic and arrived at 40 km in 117 s. With increasing distance from the vent the shock wave gradually detached from the surge. The shock led the surge by several seconds at 10 km and by about 200 s at 40 km. The ash flow followed the shock and surge by 1 min to several minutes.

This scenario can be developed in more detail for hazard evaluations at different points around the Valles volcano, and similar ones for other volcanoes may also be generated. The effect of topography on the blast runout for different locations around the volcano is especially critical where the slope of the energy line is minimal (column collapse heights small in comparison with topographic reliefs).

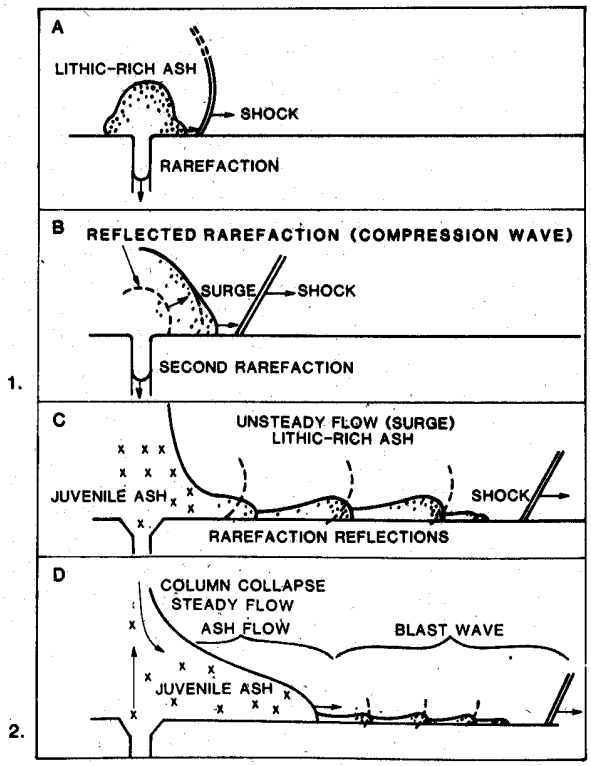

Fig. 17. Development stages of a Plinian eruption where during the initial minutes (1) a vertical shock wave forms and diffracts around the vent rim to form a weak horizontal shock (Figure 17*a*). The ash cloud following the shock is accelerated by emergence of a compression wave from the vent resulting from the reflected rarefaction (Figure 17*b*). After several rarefaction reflections the surge shows several pulses behind the leading shock (Figure 17*c*). Several minutes later a stabilized steady flow develops in the vent (2) and an ash flow initiates owing to gravitational instability of the vertical eruption cloud. The ash flow follows the blast wave (shown as the sequence including a shock wave and surge).

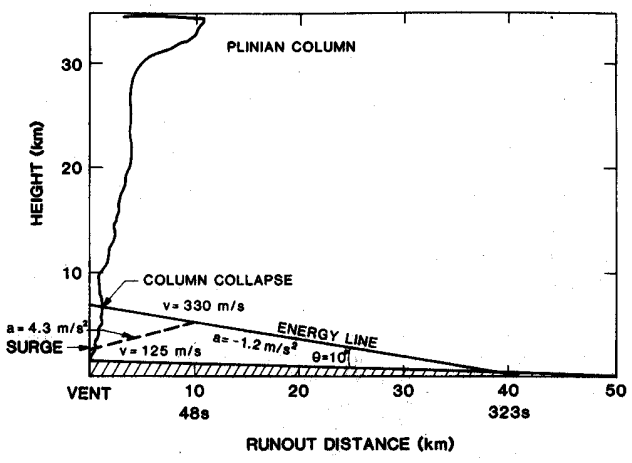

Fig. 16. Generalized energy line for the theoretical blast eruption initiating emplacement of the Bandelier Tuff, assuming a maximum runout distance of 40 km. Calculated height of the Plinian column is greater than 30 km with collapse of the column from 5 km. Maximum speed of the surge is reached after 48 s of accelerating travel from the vent area. From 48 s (10 km) to 323 s the surge decelerates from sound speed to a stop at 40 km. Note that in this visualization of surge runout the following ash flow is initiated by column collapse and follows a similar energy line.

CONCLUSIONS

Large caldera-forming eruptions display phenomena that can be explained by shock tube physics and hydrodynamic calculations, as has been demonstrated using the implicit multifield Eulerian computer method. This approach, applied to an eruption such as the one which emplaced the Bandelier Tuff and accompanied the collapse of the Valles caldera, describes the pertinent aspects of the initiation of the ash flow emplacement associated with Plinian eruption. The eruption of ash flows from a near-surface, volatile-rich magma chamber usually begins after the initial pumice falls with a catastrophic vent failure and widening and is preceded by generation of a shock wave that propagates at supersonic speed upward and sonic speed horizontally. The shock adiabatically compresses the air to pressures of several or tens of atmospheres thereby heating it to several hundred degrees centigrade. Directly behind the shock, ash particles accelerate out of the vent. Horizontally moving ash initially travels at subsonic speed and is accelerated to near the sound speed as a surge by a secondary compression wave which arrives after the interval (tens of seconds) needed for the reflected rarefaction to exit the vent. The initial blast phenomenology consists of a complicated two-phase flow originating in, and moving out of the vent. We predict that the initial moments of a large ash flow eruption consist sequentially of a shock wave, followed in several to tens of seconds by a surge which pulsates in velocity and density, and finally after about 1 min an ash flow. Figure 17 schematically depicts our conclusions.

Our description can be quantified by applying numerical hydrodynamic methods to an energy line model, a topic for future work. First-order analysis of the calculated shock wave strength shows a correlation with the magnitude of the eruptive volume. Therefore a large Plinian eruption such as the Jemez Valles may have generated a blast wave at least 2 orders of magnitude greater than that of Mount St. Helens. A semiquantitative combination of numerical hydrodynamic results with energy line considerations based upon preeruptive stratigraphy and topography allows formulation of a hazard analysis of destructive blast phenomena associated with explosive eruptions. When fully three-dimensional methods become practical, these methods can determine zones of relative danger for both loss of life and environmental destruction.

Acknowledgments. The shock tube and computer modeling aspects of this paper were initiated and suggested in 1975 by Thomas R. McGetchin; posthumous coauthorship only incompletely reflects his contributions. His keen insight and applications of hydrodynamics to eruptive mechanisms inspired many workers in volcanology at Los Alamos as well as around the world. This work, although long in gestation, is stimulating new, ongoing research in application of hydrocodes to volcanic phenomena. We benefited by discussion and support of many co-workers. Michael Sheridan early recognized the significance of the KACHINA application and strongly advocated its development. Susan Kieffer has continued to encourge our attempts at physical analysis of geologic processes. Grant Heiken and Stephen Self offered stimulating discussions and have improved the manuscript. Lionel Wilson provided a thoughtful review. Los Alamos National Laboratory is operated by the University of California for the U.S. Department of Energy.

REFERENCES

Amsden, A. A., and F. H. Harlow, KACHINA: An eulerian computer program for multifield fluid flows, *Rep. LA-5680*, 134 pp., Los Alamos Natl. Lab., Los Alamos, N. Mex., 1974.

Bailey, R. A., G. B. Dalrymple, and M. A. Lanphere, Volcanism, structure, and geochronology of Long Valley caldera, Mono County, California, *J. Geophys. Res.*, *81*, 725–744, 1976.

Bennett, F. D., Vaporization waves in explosive volcanism, *Nature*, *234*, 538–539, 1971.

Burnham, C. W., J. R. Holloway, and N. F. Davis, Thermodynamic properties of water to 1,000°C and 10,000 bars, *Spec. Pap. Geol. Soc. Am.*, *132*, 96 pp., 1969.

Christiansen, R. L., and H. R. Blank, Jr., Volcanic stratigraphy of the Quaternary rhyolite plateau in Yellowstone National Park, *U.S. Geol. Surv. Prof. Pap.*, *729-B*, 18 pp., 1972.

Dondanville, R. F., Geological characteristics of the Valles caldera geothermal system, New Mexico, *Geotherm. Res. Counc. Trans.*, *2*, 157–160, 1978.

Eichelberger, J. C., and D. B. Hayes, Magmatic model for the Mount St. Helens blast of May 18, 1980, *J. Geophys. Res.*, *87*, 7727–7738, 1982.

Fink, J. H., Structure and emplacement of a rhyolitic obsidian flow: Little Glass Mountain, Medicine Lake highlands, northern California, *Geol. Soc. Am. Bull.*, *94*, 362–380, 1983.

Fisher, R. V., Models for pyroclastic surges and pyroclastic flows, *J. Volcanol. Geotherm. Res.*, *6*, 305–318, 1979.

Gardner, J. N., Petrogenesis of the Jemez Mountains volcanic field (abstract), *Eos Trans. AGU*, *63*, 1131, 1982.

Gardner, J. N., Tectonic controls of petrogenesis, Jemez volcanic field, New Mexico, *Geol. Soc. Am. Abstr. Programs*, *15*, 380–381, 1983.

Glasstone, S., and P. J. Dolan, *The Effects of Nuclear Weapons*, 3rd ed., U.S. Department of Defense and U.S. Department of Energy, Washington, D. C., 1977.

Goff, F., Subsurface structure of Valles caldera, A resurgent cauldron in northern New Mexico, *Geol. Soc. Am. Abstr. Programs*, *15*, 381, 1983.

Harlow, F. H., and A. A. Amsden, A numerical fluid dynamics calculation method for all flow speeds, *J. Comput. Phys.*, *8*, 197, 1971.

Harlow, F. H., and A. A. Amsden, Numerical calculation of multiphase fluid flow, *J. Comput. Phys.*, *17*, 19–52, 1975.

Helgeson, H. C., and D. H. Kirkham, Theoretical prediction of the thermodynamic behavior of aqueous electrolytes at high pressure and temperatures, I, Summary of the thermodynamic/electrostatic properties of the solvent, *Am. J. Sci.*, *274*, 1089, 1974.

Hildreth, W., The Bishop tuff: Evidence for the origin of compositional zonation in silicic magma chambers, *Spec. Pap. Geol. Soc. Am.*, *180*, 43–75, 1979.

Hirt, C. W., Heuristic stability theory for finite difference equations, *J. Comput. Phys.*, *2*, 339, 1968.

Hoblitt, R. P., D. C. Miller, and J. W. Vallance, Origin and stratigraphy of the deposit produced by the May 18 directed blast, *U.S. Geol. Surv. Prof. Pap.*, *1250*, 401–419, 1981.

Hsü, K. J., Catastrophic debris streams (Sturzstrom) generated by rock falls, *Geol. Soc. Am. Bull.*, *86*, 129–140, 1975.

Kieffer, S. W., Sound speed in liquid-gas mixtures: Water-air and water-steam, *J. Geophys. Res.*, *82*, 2895–2904, 1977.

Kieffer, S. W., Fluid dynamics of the May 18 blast at Mount St. Helens, *U.S. Geol. Surv. Prof. Pap.*, *1250*, 379–400, 1981.

Knapp, R. B., and J. E. Knight, Differential thermal expansion of pore fluids: Fracture propagation and microearthquake production in hot pluton environments, *J. Geophys. Res.*, *82*, 2515–2522, 1977.

Lirer, L., T. Pescatore, B. Booth, and G. P. L. Walker, Two Plinian pumice-fall deposits from Somma-Vesuvius, Italy, *Geol. Soc. Am. Bull.*, *84*, 759–772, 1973.

Livshits, L. D., and L. G. Bolkhoritinov, Weak shock waves in the eruption column, *Nature*, *267*, 420–421, 1977.

MacDonald, G. A., *Volcanoes*, 510 pp., Prentice-Hall, Englewood Cliffs, N. J., 1972.

Malin, M. C., and M. F. Sheridan, Computer-assisted mapping of pyroclastic surges, *Science*, *217*, 637–640, 1982.

McGetchin, T. R., and G. W. Ullrich, Xenoliths in maars and diatremes with inferences for the moon, Mars, and Venus, *J. Geophys. Res.*, *78*, 1833–1853, 1973.

Miles, E. R. C., *Supersonic Aerodynamics, an Introduction*, Dover, New York, 1950.

Minakami, T., On the distribtuion of volcanic ejecta: The distribution of Mt. Asama pumice in 1783, II, *Bull. Earthquake Res. Inst*, *20*, 93–105, 1942.

Moore, J. G., and T. W. Sisson, Deposits and effects of the May 18 pyroclastic surge, *U.S. Geol. Surv. Prof. Pap.*, *1250*, 421–438, 1981.

Nairn, I. A., Atmospheric shock waves and condensation clouds from Ngauruhoe explosive eruptions, *Nature*, *259*, 190–192, 1976.

Pai, S. I., Y. Hsu, and J. A. O'Keefe, Similar explosive eruptions of lunar and terrestrial volcanoes, *Proc. Lunar Planet. Sci. Conf. 9th*, 1485–1508, 1978.

Perret, F. A., The eruption of Mt. Pelee, 1929–1932, *Carnegie Inst. Washington Publ., 458*, 125 pp., 1935.
Rosi, M., and R. Santacroce, The A.D. 472 "Pollena" eruption: Volcanological and petrological data for this poorly-known, Plinian-type event at Vesuvius, *J. Volcanol. Geotherm. Res., 17*, 249–271, 1983.
Sandford, M. T., II, E. M. Jones, and T. McGetchin, Hydrodynamics of caldera-forming eruptions, *Geol. Soc. Am. Abstr. Programs, 7*, 1257, 1975.
Segar, R. L., Quantitative gravity interpretation, Valles caldera area, New Mexico, open file rep., 14 pp., Union Oil Co. Geotherm. Div., Santa Rosa, Calif., 1974.
Self, S., and J. V. Wright, Dynamics of the Bandelier Plinian eruptions and implications for the generation of large volume ignimbrites (abstract), *Eos Trans. AGU, 62*, 1085, 1981.
Self, S., L. Wilson, and I. Nairn, Vulcanian eruption mechanisms, *Nature, 277*, 440–443, 1979.
Shapiro, A. H., *The Dynamics and Thermodynamics of Compressible Fluid Flow*, vols. 1 and 2, 1185 pp., John Wiley, New York, 1953.
Sheridan, M. F., Emplacement of pyroclastic flows: A review, *Spec. Pap. Geol. Soc. Am., 180*, 125–136, 1979.
Sheridan, M. F., and K. H. Wohletz, Hydrovolcanism: Basic considerations and review, *J. Volcanol. Geotherm. Res., 17*, 1–29, 1983.
Sheridan, M. F., F. Barberi, M. Rosi, and R. Santacroce, A model for Plinian eruptions of Vesuvius, *Nature, 284*, 282–285, 1981.
Smith, R. L., Ash flows, *Geol. Soc. Am. Bull., 71*, 795–842, 1960.
Smith, R. L., Ash flow magmatism, *Spec. Pap. Geol. Soc. Am., 180*, 5–27, 1979.
Smith, R. L., and R. A. Bailey, Structural evolution of the Valles caldera, New Mexico, *U.S. Geol. Surv. Prof. Pap., 424-D*, 1961.
Smith, R. L., and R. A. Bailey, Resurgent cauldrons, *Mem. Geol. Soc. Am., 116*, 613–662, 1968.
Smith, R. L., and H. R. Shaw, Igneous related geothermal systems, *U.S. Geol. Surv. Circ., 726*, 58–83, 1975.
Smith, R. L., R. A. Bailey, and C. S. Ross, Geologic Map of the Jemez Mountains, New Mexico, *Map I-571*, U.S. Geol. Surv., Washington, D. C., 1970.
Soo, S. L., *Fluid Dynamics of Multiphase Systems*, Blaisdell Publications, Waltham, Mass., 1967.
Sparks, R. S. J., Grain size variations in ignimbrites and implications for the transport of pyroclastic flows, *Sedimentology, 23*, 147–188, 1976.
Sparks, R. S. J., The dynamics of bubble formation and growth in magmas: A review and analysis, *J. Volcanol. Geotherm. Res., 3*, 1–37, 1978.
Sparks, R. S. J., S. Self, and G. P. L. Walker, Products of ignimbrite eruptions, *Geology, 4*, 115–118, 1973.
Sparks, R. S. J., L. Wilson, and G. Hulme, Theoretical modeling of the generation, movement, and emplacement of pyroclastic flows by column collapse, *J. Geophys. Res., 83*, 1727–1739, 1978.
Thorarinsson, S., and G. E. Sigvaldason, The Hekla eruption of 1970, *Bull. Volcanol., 36*, 269–288, 1972.
Tuttle, O. F., and N. L. Bowen, Origin of granite in the light of experimental studies in the system $NaAlSi_3O_8$-$KalSi_3O_8$-SiO_2-H_2O, *Mem. Geol. Soc. Am., 74*, 1958.
Walker, G. P. L., The Taupo pumice: Product of the most powerful known (ultraplinian) eruption, *J. Volcanol. Geotherm. Res., 8*, 69–94, 1980.
Walker, G. P. L., Plinian eruptions and their products, *Bull. Volcanol., 44*, 223–240, 1981.
Walker, G. P. L., and R. Croasdale, Two Plinian eruptions in the Azores, *J. Geol. Soc. London, 127*, 17–55, 1971.
Wilson, L., R. S. J. Sparks, and G. P. L. Walker, Explosive volcanic eruptions, IV, The control of magma properties and conduit geometry on eruption column behavior, *Geophys. J. R. Astron. Soc., 63*, 117–148, 1980.
Wohletz, K. H., and M. F. Sheridan, A model of pyroclastic surge, *Spec. Pap. Geol. Soc. Am., 180*, 177–194, 1979.
Wright, J. K., *Shock Tubes*, Methuen, London, 1967.
Zel'dovich, Ya. B., and Yu. P. Razier, Physics of shock waves and high temperature hydrodynamic phenomena, edited by W. D. Hayes and R. F. Probstein, vols. I and II, 916 pp., Academic, New York, 1966.

E. M. Jones, M. T. Sandford II, and K. H. Wohletz, Los Alamos National Laboratory, Earth and Space Sciences Division, Geology, ESS-1/D461, Los Alamos, NM 87545.

(Received August 22, 1983;
revised February 8, 1984;
accepted March 1, 1984.)